Hu, G., Cho, H., Wan, H., Ohtaki, H., On the tensile strength of brittle materials with a consideration of Poisson's ratios.
International Symposium on the Fusion Technology of Geosystem Engineering, Rock Engineering and Geophysical Exploration
Seoul, Korea, Nov. 18-19, 2003

On the tensile strength of brittle materials with a consideration of Poisson's ratios

Guoming Hu[1], Heechan Cho[1], Hui Wan[2], Hideyuki Ohtaki[2]
[1]Seoul National University, Seoul, Korea, [2] Saitama University, Saitama, Japan

Abstract: The influence of Poisson's ratio on the tensile strength of brittle materials is neglected in many studies. When brittle materials are loaded in compression or impact, substantial tensile stresses are induced within the materials. These tensile stresses are responsible for splitting failure of the materials. In this paper, the state of stress in a spherical particle due to two diametrically opposed forces is analyzed theoretically. A simple equation for the state of stress at the center of the particle is obtained. An analysis of the distribution of stresses along the z-axis due to distributed pressures and concentrated forces, and on diametrically horizontal plane due to concentrated forces, shows that it is reasonable to propose the tensile stress at the center of the particle at the point of failure as a tensile strength of the particle. Moreover, the tensile strength is a function of the Poisson's ratio of the material. As the state of stress along the z-axis in an irregular specimen tends to be similar to that in a spherical particle compressed diametrically with the same force, this tensile strength has some validity for irregular particles as well. Therefore, it can be proposed as the tensile strength for brittle materials generally. The effect of Poisson's ratio on the tensile strength is discussed.

1. Introduction

When a particle is subjected to a load, the nature of the stress field around and within brittle materials, the material properties, and the size and distribution of micro-flaws within the materials govern the size and shape distribution of the fragments and the surface area produced. The exact description of the micro-flaw pattern would represent a meaningless task in view of the fact that the details of flaw pattern will to a significant degree differ from one sample to the other. But the nature of the stress field is exactly determined by the contact features and the material properties (Briggs and Bearman, 1996). When brittle materials are loaded in compression or impact, and very large compressive stresses are generated at the contact point, substantial tensile stresses are also induced within the particle, and failure eventually occurs by splitting the particle along a plane or planes that run parallel to the direction of load application.

Awareness of these facts has lead to a resurgence of interest in tensile strength of brittle materials. Tensile strength has been studied by many investigators to analyze the impact damage and compressive damage in brittle materials. Here one can cite the works of Andrews and Kim (1998), Camacho and Ortiz (1996), Butenuth (1997), and Hiramustu and Oka (1966). Tavares and King (1998) used the formula of tensile strength obtained by Hiramustu and Oka (1966) to estimate the strength of a particle subject to impact on UFLC (The Ultrafast Load Cell). Yashima *et al.* (1987) have applied the same formula to obtain the specific fracture energy for particle breakage.

A number of methods exist to fail brittle material in tension. In some, specimens are loaded by directly induced tension, as in the direct test for tension; in others, tension is induced indirectly via compression, as in point load test and line load test. In general, the experimental results obtained by indirect tensile tests are not strictly comparable with those from direct tensile tests, because of the existence of a compressive component that may be far greater in magnitude than the induced tensile stress, and whose influence on failure cannot therefore be ignored. Since the mode of indirect tensile failure is common in many industry application, as, for instance, in comminution, the tensile nature of failure in indirect tensile tests is an advantage rather than a drawback.

For a cylinder loaded by two equal and opposite line forces P/t acting along a diameter, the state of stress at any point along this diameter is given by the principal stresses with a constant tensile stress superimposed by a varying compressive stress, as described by Timoshenko and Goodier (1987) and many others. The constant tensile stress is given by:

$$\sigma_t = 2P/(\pi Dt) \tag{1}$$

where D is the diameter of the cylinder, t is the length of line force.

In the case of sphere, Hiramustu and Oka (1966) obtained the stress distribution from Lengendre's polynomial in polar spherical coordinates. The tensile strength they found is indicated by the tensile stress at the center of the particle at the point of failure and expression for the tensile strength is given by:

$$\sigma_t = 2.8P/(\pi D^2) \tag{2}$$

A general conclusion can be drawn concerning indirect tensile tests (Broch and Franklin, 1972): The maximum tensile stress, occurring at the center of the specimen, is related to the applied force P, the distance between the point forces, D, by the expression of $\sigma_t=kP/D^2$ in the point load tests; it also depends on the length of line loading, t, by the expression of $\sigma_t=kP/(Dt)$ as in the line load tests, where k is a constant depending on the loading type and the geometry of the specimen.

In the mechanics analysis, it is well known that some solutions for stress or displacement fields are dependent on Poisson's ratios of materials, while other solutions are independent on Poisson's ratios of materials. However, since many engineering materials have Poisson's ratios very close to 0.3, such dependence has received comparatively little attention. The above conclusion concerning indirect tensile tests does not consider the effect of Poisson's ratio on the tensile strength of brittle materials. Brittle materials exhibit a considerably varying range of Poisson's ratio, for example, Poisson's ratios of rocks range for zero to 0.5 (Lama and Vutukuri, 1978). Moreover, a number of minerals and rocks with micro-cracks (Homand-Etienne and Houpert, 1989, Nur and Simmons, 1969) were discovered to have negative Poisson's ratios. Hence the effect of Poisson's ratio on the tensile strength of brittle materials deserves re-examination within the context of mechanics analysis.

In this paper, a theoretical approach is made to the tensile strength of brittle materials. Through the analysis of the state of stress in a spherical particle due to two diametrically opposed forces, it is found reasonable to propose the tensile stress at the center of the particle at the point of failure as a tensile strength of the particle. This tensile strength is also valid for irregular particles and reflects the influence of Poisson's ratio, which was not taken into account in the previous studies.

2. Problem Formulation

Stresses for any point within a sphere due to two opposite concentrated forces

As shown in Fig. 1, stresses at point A within a half-space produced by a concentrated point force acting on the half-space are given by (Timoshenko and Goodier, 1987):

$$\sigma_r = \frac{P}{2\pi\rho^2}\left[-\frac{3r^2 z}{\rho^3} + \frac{(1-2\mu)\rho}{\rho+z}\right] \tag{3}$$

$$\sigma_\theta = \frac{(1-2\mu)P}{2\pi\rho^2}\left[\frac{z}{\rho} - \frac{\rho}{\rho+z}\right] \tag{4}$$

$$\sigma_z = -3Pz^3/(2\pi\rho^5) \tag{5}$$

$$\tau_{rz} = -3rPz^2/(2\pi\rho^5) \tag{6}$$

where σ_r is radial stress, σ_θ is circumferential stress, σ_z is longitudinal stress, τ_{rz} is shear stress, μ is Poisson's ratio, and ρ is the distance from point A to the original O.

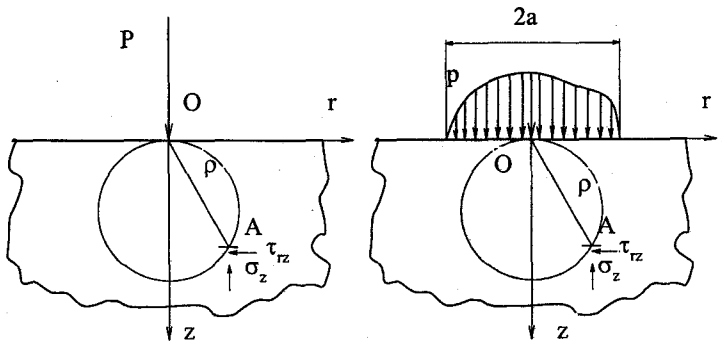

Fig. 1. A concentrated force or a distribution pressure acting on a half-space.

The stresses acting on an elemental area *mn* perpendicular to the z-axis within a spherical particle due to two equal and opposite concentrated forces, as shown in Fig. 2, can be obtained by superposing the stresses due to the two concentrated forces P acting on O_1 and O_2, using Eq(3)~Eq(6):

$$\sigma_r = \sigma_{r,1} + \sigma_{r,2} = \frac{P}{2\pi\rho_1^2}[-\frac{3r^2(R-z)}{\rho_1^3} + \frac{(1-2\mu)\rho_1}{\rho_1+R-z}] + \frac{P}{2\pi\rho_2^2}[-\frac{3r^2(R+z)}{\rho_2^3} + \frac{(1-2\mu)\rho_2}{\rho_2+R+z}] \tag{7}$$

$$\sigma_\theta = \sigma_{\theta,1} + \sigma_{\theta,2} = \frac{(1-2\mu)P}{2\pi\rho_1^2}[\frac{(R-z)}{\rho_1} - \frac{\rho_1}{\rho_1+R-z}] + \frac{(1-2\mu)P}{2\pi\rho_2^2}[\frac{(R+z)}{\rho_2} - \frac{\rho_2}{\rho_2+R+z}] \tag{8}$$

$$\sigma_z = \sigma_{z,1} + \sigma_{z,2} = -\frac{3P}{2\pi}[\frac{(R-z)^3}{\rho_1^5} + \frac{(R+z)^3}{\rho_2^5}] \tag{9}$$

$$\tau_{rz} = \tau_{rz,1} + \tau_{rz,2} = -\frac{3rP}{2\pi}[\frac{(R-z)^2}{\rho_1^5} - \frac{(R+z)^2}{\rho_2^5}] \tag{10}$$

where R is radius of the particle, ρ_1, ρ_2 are the distances of point A within the particle to O_1, O_2 respectively, and second subscripts refer to the stresses caused by the forces at O_1 and O_2 respectively.

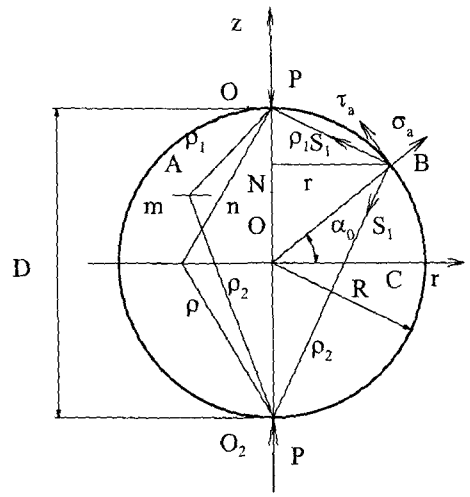

Fig. 2. Two concentrated forces acting on a spherical particle.

Stresses on the boundary of the sphere due to two opposite concentrated forces

The longitudinal and shear stresses σ_z and τ_{rz}, which act on elemental area *mn* within the sphere, are independent of Poisson's ratio. At a point B on the surface of the particle, from Eq(9) and Eq(10), the ratios of longitudinal and shear components of the stress on this element are $\sigma_{z,1}/\tau_{rz,1}=(R-z)/r$ and $\sigma_{z,2}\tau_{rz,2}=(R+z)/r$. The resultant stresses S_1 and S_2 of the longitudinal and shear stresses acting on a plane intersecting the surface of the particle and perpendicular to the z-axis are:

$$S_1 = S_2 = (\sigma_{z,1}^2 + \tau_{rz,1}^2)^{1/2} = (\sigma_{z,2}^2 + \tau_{rz,2}^2)^{1/2} = 3P/(8\pi R^2) = const \tag{11}$$

So for any point B on the spherical surface, the resultant stresses on the horizontal plane are compressive and constant, and of value $3P/(8\pi R^2)$, and the directions of the resultant stresses are towards O_1 and O_2 respectively.

Because of the presence of the shear stress τ_{rz}, σ_r and σ_z are not principal stresses, although σ_θ is a principal stress as $\tau_{r\theta}=\tau_{z\theta}=0$. So it can be seen that S_1 and S_2 are not principal stresses and that the principal stress does not act in a radial direction with respective to O, nor are the surfaces of constant principal shear stress spherical.

The normal and shear stresses σ_α and τ_α for any point B on the surface of the particle can be written as:

$$\sigma_\alpha = \sigma_r \frac{R^2-z^2}{R^2} + \sigma_z \frac{z^2}{R^2} - 2\tau_{rz}\frac{z(R^2-z^2)^{1/2}}{R^2} \tag{12}$$

$$\tau_\alpha = (\sigma_r - \sigma_z)\frac{z(R^2 - z^2)^{1/2}}{R^2} + \tau_{rz}\frac{R^2 - 2z^2}{R^2} \tag{13}$$

Radial stress σ_α and shear stress τ_α as they depend on the value of z are shown in Fig. 3. As can be seen, σ_α and τ_α along the boundary are not uniformly distributed. Therefore a general approach that frees the spherical boundary of the sphere from stress as is possible to free the circular boundary from stress in the case of cylindrical bodies cannot be used. However, τ_α equals zero at the circular boundary on the horizontal diametrical plane, so σ_α is a principal stress at this circular boundary. In this special case, we can obtain the state of stress by an approach similar to that in the case of cylindrical bodies.

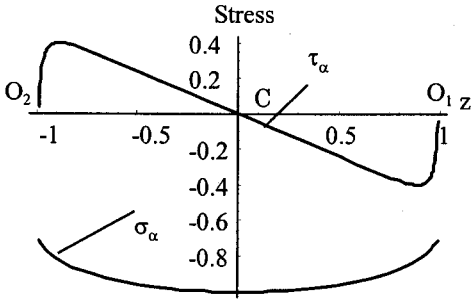

Fig. 3. The radial stress and shear stress on the boundary surface.

Stresses on the horizontal diametrical plane due to two opposite concentrated forces

The boundary of the particle is free from external forces except at two points where the opposite concentrated forces are exerted. The radial stress σ_α and shear stress τ_α are due to the stresses of σ_r, σ_z and τ_{rz}, so the stresses at any point in the particle are therefore obtained by superposing $-\sigma_r^{Boundary}$, $-\sigma_z^{Boundary}$ and $-\tau_{rz}^{Boundary}$ on the stresses produced by the two concentrated forces P. However, it is difficulty to minimize the shear stress on the surface and to satisfy the symmetry property of the shear stress along the z-axis. This difficulty makes an analysis based on the superposition principle invalid in the general case.

As shown in Fig. 3, the shear stress τ_α equals zero at point C, exact solutions for the state of stress on the horizontal diametrical plane can be obtained. From symmetry it can be concluded that there will be no shear stress on the horizontal diametrical plane. The state of stress along the z-axis is uniform bi-axial tension with superimposed longitudinal compression. Substituting z=0, r=R, and ρ_1=ρ_2=$2^{1/2}R$ into Eq(7) and Eq(9) respectively, the radial and longitudinal stresses at any point C at the circular boundary on the horizontal diametrical plane are obtained and given by:

$$\sigma_r^{Boundary} = 2\left((1-2\mu)\frac{\sqrt{2}}{\sqrt{2}+1} - \frac{3}{2\sqrt{2}}\right)\frac{P}{\pi D^2} \tag{14}$$

$$\sigma_z^{Boundary} = -3\sqrt{2}P/(2\pi D^2) \tag{15}$$

Stresses at any point on the horizontal diametrical plane comprise the superposition of the stresses σ_r, σ_θ and σ_z due to two concentrated forces P given by Eq(8) to Eq(10) together with $-\sigma_r^{Boundary}$, $-\sigma_r^{Boundary}$ and $-\sigma_z^{Boundary}$ respectively and are expressed by:

$$\sigma_r = \frac{P}{\pi D^2}\left\{\frac{4R^2}{\rho^2}\left[-\frac{3r^2R}{\rho^3} + \frac{(1-2\mu)\rho}{\rho+R}\right] - 2\left((1-2\mu)\frac{\sqrt{2}}{\sqrt{2}+1} - \frac{3}{2\sqrt{2}}\right)\right\} \tag{16}$$

$$\sigma_\theta = \frac{P}{\pi D^2}\left\{\frac{4R^2(1-2\mu)}{\rho^2}\left[\frac{R}{\rho} - \frac{\rho}{\rho+R}\right] - 2\left((1-2\mu)\frac{\sqrt{2}}{\sqrt{2}+1} - \frac{3}{2\sqrt{2}}\right)\right\} \tag{17}$$

$$\sigma_z = -\frac{P}{\pi D^2}\left[\frac{12R^5}{\rho^5} - \frac{3\sqrt{2}}{2}\right] \tag{18}$$

$\sigma_r^{Boundary}$ and $\sigma_z^{Boundary}$ free the circular boundary on the horizontal diametrical plane from longitudinal stress and radial stress.

Stresses along the z-axis due to distributed pressures

Referring back to Fig. 1, a distribution pressure is applied on a circular region of radius a on the surface of the half-space. Because of the complex nature of the equations for stresses at a general point, it is considered valuable to pay attention to the stresses along the z-axis. This is helpful from the practical point of view because the severest state of stress occurs there.

The stresses along the z-axis due to a uniformly distributed pressure are given by (Johnson, 1985):

$$\sigma_r = \sigma_\theta = -p\left(\frac{1+2\mu}{2} - \frac{(1+\mu)z}{(a^2+z^2)^{1/2}} + \frac{z^3}{2(a^2+z^2)^{3/2}}\right) \tag{19}$$

$$\sigma_z = -p(1-z^3/(a^2+z^2)^{3/2}) \tag{20}$$

where $p=P/(\pi a^2)$, and a is radius of the region where the pressure is applied. While the stresses along the z-axis due to Hertz's distribution pressure are given by:

$$\sigma_r / p_0 = \sigma_\theta / p_0 = -(1+\mu)\{1-(z/a)\arctan(a/z)\} + 0.5(1+z^2/a^2)^{-1} \tag{21}$$

$$\sigma_z / p_0 = -(1+z^2/a^2)^{-1} \tag{22}$$

where $p_0 = 3P/(2\pi a^2)$.

Consider the particle shown in Fig. 4, which is being subjected to a combination of diametrically opposed distributed pressures with total load P. The state of stress at point N along the z-axis is made up of three contributions: (i) the stress due to the distributed pressure on contact at O_1; (ii) the stress due to the distributed pressure at O_2, and (iii) the stress by superposing an opposite stress due to the two concentrated forces P acting on the boundaries of the particle, given by Eq(14) to Eq(15).

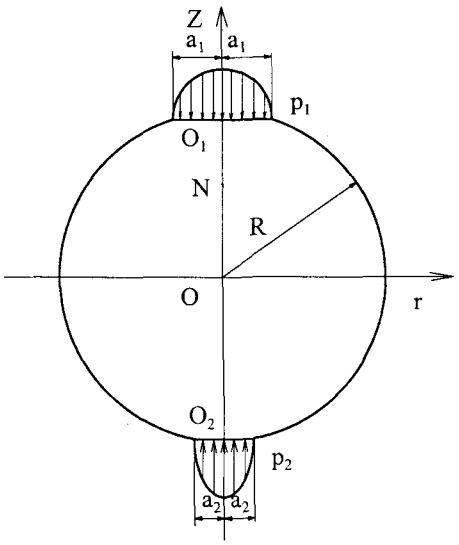

Fig. 4. Two distribution pressures acting on a particle.

3. Results and Discussion

The state of stress at the center of the particle

The state of stress at the center of the particle due to two opposite concentrated forces

The state of stress on the horizontal diametrical plane due to two opposite concentrated forces as it depends on the value of r is shown in Fig. 5. As can be seen, the maximum compressive and tensile stresses on the horizontal diametrical plane due to two opposite concentrated forces are at the center of the sphere, where:

$$\sigma_{r,o} = \sigma_{\theta,o} = \frac{P}{\pi D^2}\left(\frac{3}{\sqrt{2}} + (1-2\mu)\frac{2}{\sqrt{2}+1}\right) \tag{23}$$

$$\sigma_{z,o} = -(12 - 3\sqrt{2}/2)P/(\pi D^2) \tag{24}$$

At the circular boundary, the radial stress and longitudinal stress vanish, but the circumferential stress exists and is given by:

$$\sigma_{\theta}^{Boundary} = (3\sqrt{2}/2 - (1-2\mu)(8-5\sqrt{2}))P/(\pi D^2) \tag{25}$$

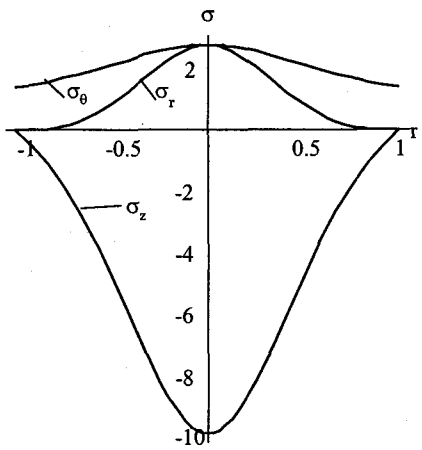

Fig. 5. The state of stress on the horizontal diametrical plane due to two opposite concentrated forces.

The state of stress at the center of the particle due to two opposite uniform pressures

The force exerted on a particle in a Brazilian test can be treated as a uniformly distributed pressure. An analytic solution in closed form of stresses at any point along the z-axis due to two opposite uniform pressures may not exist except at the center of the particle. Combining Eq(19) and Eq(20) with Eq(14) and Eq(15), we obtain the stresses at the center of the particle due to two opposite uniform distribution pressures. They are:

$$\sigma_{r,o} = \sigma_{\theta,o} = \frac{P}{\pi D^2}\left(-\frac{8R^2}{a^2}\left(\frac{1+2\mu}{2} - (1+\mu)\frac{(R^2-a^2)^{1/2}}{R} + 0.5\frac{(R^2-a^2)^{3/2}}{R^3}\right) - C_0\right) \tag{26}$$

$$\sigma_{z,o} = -\frac{P}{\pi D^2}\left(\frac{8R^2}{a^2}\left(1 - \frac{(R^2-a^2)^{3/2}}{R^3}\right) - 3\sqrt{2}/2\right) \tag{27}$$

where $C_0 = 2((1-2\mu)\sqrt{2}/(\sqrt{2}+1) - 3/(2\sqrt{2}))$.

The state of stress at the center of the particle due to two opposite Hertz's pressures

The forces exerted on a particle in slow compression and double impact can be treated as two opposite Hertz's distribution pressures. Combining Eq(21) and Eq(22) with Eq(14) and Eq(15), we obtain the stresses at the center of the particle due to two opposite Hertz's distribution pressures. The tensile stress at the center of the particle is given by:

$$\sigma_{r,o} = \sigma_{\theta,o} = \frac{P}{\pi D^2}\left(\frac{6R^2}{a^2}\left(-2(1+\mu)\left(1 - \frac{(R^2-a^2)^{1/2}}{a}\arctan\frac{a}{(R^2-a^2)^{1/2}}\right) + \frac{a^2}{R^2}\right) - C_0\right) \tag{28}$$

It is interesting to see that the longitudinal stress is the same as in the case of two opposite concentrated forces, and is also given by Eq(24).

The effect of Poisson's ratio upon the tensile strength

For the three loading conditions, it can be seen that $\sigma_{r,o}$ and $\sigma_{\theta,o}$ are tensile stresses and their magnitudes depend on Poisson's ratio, while $\sigma_{z,o}$ is a compressive stress and its magnitude does not depend on Poisson's ratio.

For the loading condition of two opposite concentrated forces, the tensile stress depending on Poisson's ratio is shown in Table 1.

For the loading condition of two opposite uniform pressures, the tensile stress $\sigma_{r,o}$ as it depends on the values of μ and a/R is shown in Table 2. It can be seen that the influence of μ on $\sigma_{r,o}$ is much stronger than that of a/R. The magnitude of $\sigma_{r,o}$ decreases as the values of μ and a/R increases. The severest stress happens when a/R tends to zero.

Table 1. Tensile stress at the center of the particle due to concentrated forces.
(The tensile stress is k multiplied by $P/(\pi D^2)$)

μ	0	0.1	0.2	0.3	0.4	0.5
k	2.94975	2.78406	2.61838	2.45269	2.28701	2.12132

Table 2. Tensile stress at the center of the particle due to uniform distribution pressures.
(The tensile stress is k multiplied by $P/(\pi D^2)$)

μ			0	0.1	0.2	0.3	0.4	0.5
a/R	0.0001	k	2.94975	2.78406	2.61838	2.45269	2.28701	2.12132
	0.01		2.9495	2.7838	2.61811	2.45241	2.28672	2.12102
	0.02		2.94875	2.78302	2.6173	2.45157	2.28585	2.12012
	0.03		2.9475	2.78172	2.61595	2.45017	2.28439	2.11862
	0.04		2.94575	2.7799	2.61405	2.44821	2.28236	2.11652
	0.05		2.94349	2.77756	2.61162	2.44569	2.27975	2.11381
	0.06		2.94074	2.77469	2.60865	2.4426	2.27655	2.11051
	0.07		2.93748	2.7713	2.60513	2.43895	2.27277	2.1066
	008		2.93372	2.76739	2.60106	2.43473	2.26841	2.10208
	0.09		2.9245	2.76295	2.59645	2.42995	2.26345	2.09695
	0.1		2.92469	2.75798	2.59129	2.4246	2.25791	2.09122

For the loading condition of two opposite Hertz's pressures, the tensile stress $\sigma_{r,o}$ depending on the values of μ and a/R is shown in Table 3. In this situation, the radius of the region of pressure is determined by the applied forces P. The influence of a/R and μ on the tensile stress $\sigma_{r,o}$ is similar to the case of two opposite uniform pressures. With the same values of P, a/R and μ, the tensile stress $\sigma_{r,o}$ due to two opposite Hertz's pressures is a little larger than that due to two opposite uniform pressures.

Table 3. Tensile stress at the center of the particle due to Hertz's distribution pressures.
(The tensile stress is k multiplied by $P/(\pi D^2)$)

μ			0	0.1	0.2	0.3	0.4	0.5
a/R	0.0001	k	2.94975	2.78406	2.61838	2.45269	2.28701	2.12132
	0.01		2.94959	2.78389	2.61818	2.45248	2.28678	2.12108
	0.02		2.94911	2.78336	2.61761	2.45186	2.28611	2.12036
	0.03		2.94831	2.78248	2.61665	2.45082	2.28499	2.11916
	0.04		2.94719	2.78124	2.6153	2.44936	2.28342	2.11748
	0.05		2.94574	2.77966	2.61357	2.44748	2.2814	2.11531
	0.06		2.94398	2.77771	2.61145	2.44519	2.27893	2.11266
	0.07		2.94189	2.77541	2.60894	2.44247	2.276	2.10953
	008		2.93947	2.77276	2.60604	2.43933	2.27262	2.1059
	0.09		2.93673	2.76974	2.60275	2.43576	2.26878	2.10179
	0.1		2.93366	2.76636	2.59907	2.43177	2.26448	2.09718

4. Conclusions

For spherical bodies, numerical calculation by Hiramatsu and Oka demonstrated that σ_r and σ_θ along the z-axis were tensile stresses and distributed fairly uniformly over the central part, about half the diameter wide, and changed to compressive stresses in the neighborhoods of the loading points. We therefore propose that the tensile

stress at the center of the particle under the three loading conditions of two opposite concentrated forces, two opposite uniform pressures and two opposite Hertz's pressures as given by Eq(23), Eq(26) and Eq(28) respectively at the point of failure can be used as the tensile strength of brittle particles, which splitting the particle along a plane that parallel to the direction of load application. This tensile strength reflects the influences of Poisson's ratio, and of the radius of the region where the distributed pressures act, which have been omitted in studies up to now.

Figure 6 shows the distributions of longitudinal stress along the z-axis of a half-space acted on by three different types of forces. It can be seen that although the stresses due to different loading are different in the neighborhoods of the loading point, as z/a increases, their difference decreases. Above z/a=2~3, they tend to the same distribution. It is reasonable to assume that the distributions of the longitudinal stress along the z-axis of a spherical particle acted by different types of forces with the same magnitude are the same beyond the neighbourhoods of the loading points. So the tensile strength obtained in one case has some validity in another case, provided that the particle is loaded by two opposite diametrical forces.

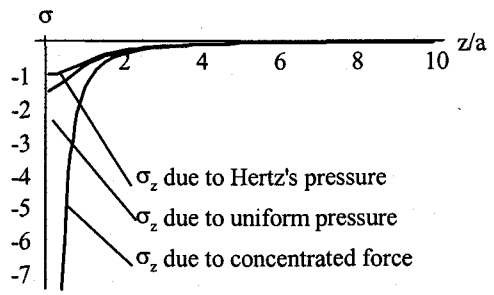

Fig. 6. Distribution of longitudinal stress along the z-axis of a half space acted on by three different types of forces.

Because the state of stress along the z-axis in an irregular specimen may be the same as that in a spherical particle compressed diametrically with the same force, the above-mentioned tensile strength can be expected to be valid for an irregular particle as well.

References

Andrews, E. W. and Kim, K. -S., 1998, Threshold conditions for dynamic fragmentation of ceramic particles, Mechanics of Materials, Vol. **29,** No. **3**, 161-180.

Briggs, C. A. and Bearman, R. A., 1996, An investigation of rock breakage and damage in comminution equipment Minerals Engineering, Vol. **9,** No. **5**, 489-497.

Broch, E. and Franklin, J. A., 1972, The point-load strength test, Int. J. Rock Mech. Min. Sci., Vol. **9**, 669-697.

Butenuth, C., 1997, Comparison of tensile strength values of rocks determined by point load and direct tension tests Rock Mechanics and Rock Engineering, Vol. **30** No. **1**, 65-72.

Camacho, G. T. and Ortiz, M., 1996, Computational modelling of impact damage in brittle materials, Int. J. Solids Structures, Vol. **33** No. **20-22**, 2899-2938.

Hiramatsu, Y. and Oka, Y., 1966, Determination of the tensile strength of rock by a compression test of an irregular test piece, Int. J. Rock Mech. Min. Sci., Vol. **3**, 89-99.

Homand-Etienne, F. and Houpert, R., 1989, Thermally induced microcracking in granites: characterization and analysis. Int. J. Rock Mech. Min. Sci & Geomech. Abstr. Vol. 26, 125-134.

Johnson, K. L., 1985, Contact Mechanics, Cambridge University Press.

Lama, R. D. and Vutukuri, 1978, Handbook on Mechanical Properties of Rocks: Testing Techniques and Results, Trans Tech Publications.

Nur, A. and Simmons, G., 1969, The effect of saturation on velocity in low porosity rocks, Earth and planet. sci. lett. Vol. 7, 183-193.

Tavares, L. M. and King, R. P., 1998, Single-particle fracture under impact loading, International Journal of Mineral Processing, Vol. **54**, 1-28.

Timoshenko, S. P. and Goodier, J. N., 1987, Theory of Elasticity, McGraw-Hill, Inc.

Yashima, S., Kanda, Y. and Sano, S., 1987, Relationships between particle size and fracture energy or impact velocity required to fracture as estimated from single particle crushing, Powder Technology, Vol. **51**, 277-282.